

Millikelvin Si-MOSFETs for Quantum Electronics

Nikolai Yurttagul,^{1,*} Markku Kainlauri,¹ Jan Toivonen,¹ Sushan Khadka,¹ Antti Kanninen,² Arvind Kumar,² Diego Subero,¹ Juha Muhonen,² Mika Prunnila,¹ and Janne S. Lehtinen^{1,†}

¹*SemiQon Technologies, Tietotie 3, 02150 Espoo, Finland*

²*University of Jyväskylä, NanoScience Center, Department of Physics, PB 35, 40014, Jyväskylä, Finland*

Large power consumption of silicon CMOS electronics is a challenge in very-large-scale integrated circuits and a major roadblock to fault-tolerant quantum computation. Matching the power dissipation of Si-MOSFETs to the thermal budget at deep cryogenic temperatures, below 1 K, requires switching performance beyond levels facilitated by currently available CMOS technologies. We have manufactured fully depleted silicon-on-insulator MOSFETs tailored for overcoming the power dissipation barrier towards sub-1 K applications. With these cryo-optimized transistors we achieve a major milestone of reaching subthreshold swing of 0.3 mV/dec at 420 mK, thereby enabling very-large-scale integration of cryo-CMOS electronics for ultra-low temperature applications.

Cryogenic CMOS holds great potential for emerging fields such as high-performance computing [1–6], space technologies [3, 7], and quantum nanoelectronics [8, 9]. Fault-tolerant quantum computation is projected to require low-noise connectivity and electronic control of up to millions of qubits at cryogenic temperatures [10], which is achievable by operating Si-CMOS integrated circuits at ultralow temperatures. Established and scalable qubit platforms typically operate below 1 K, where current cryo-CMOS power metrics would overwhelm the cooling power of available refrigeration methods, usually in the range of a few μW to several mW [11]. Scaling down power dissipation of CMOS electronics accordingly requires reducing both static power loss, by reducing off-state leakage currents, as well as dynamic power loss, by reducing the supply voltage V_{dd} . The ability to reduce both simultaneously is limited by the diffusive subthreshold conductance of a MOSFET, quantified by the subthreshold swing $SS = dV_g/d(\log_{10}I_d)$, with the drain current I_d and the gate-voltage V_g [12]. The lower limit of SS is set by the extent of thermal excitations of conduction electrons at temperature T , approximated by the lower thermionic limit $SS(T) = \ln(10)k_B T/e$, with the Boltzmann constant k_B , and elementary charge e .

However, the thermionic limit of switching is not reached in real MOSFETs, as subgap states, which start to dominate the subthreshold current below a characteristic limit temperature, cause a freeze-out of the sub-threshold conductance [13–18]. This effect becomes more significant towards ultra-low temperatures, imposing an unfavorable scaling for operating cryo-CMOS electronics. Around liquid ^4He temperatures (4.2 K) measured values for SS are usually well above 10 mV/dec for a wide variety of MOSFET types, which is an order of magnitude larger than the thermionic limit $SS(4\text{ K}) = 0.8\text{ mV/dec}$. Lowest reported values for foundry fabricated FD-SOI MOSFETs

are not lower than 5–7 mV/dec at 4 K [14, 19] and further cooling towards millikelvin temperatures has shown no significant improvement so far [9, 13–18, 20], except for a recent study [21] where a further drop of SS was found below 100 mK after initial saturation.

Apart from a sharper turn-on, other key MOSFET and circuit metrics improve towards lower temperatures, such as reduced wire delays, increased on-current due to increased carrier mobility, lower gate leakage currents, and higher charge retention times. Challenges originate from quantum effects [22–24] and a thermal shift in threshold voltage [5]. The latter can be controlled in FD-SOI MOSFETs, making it an attractive technological platform for cryo-CMOS [19]. Additionally, in fully depleted channels one can profit from a high mobility and possibly a reduced localization of charge carriers [25].

Accounting for this, we experimentally evaluate FD-SOI MOSFETs, fabricated on a custom CMOS pilot-line for manufacturing monolithically integrated cryo-CMOS ICs

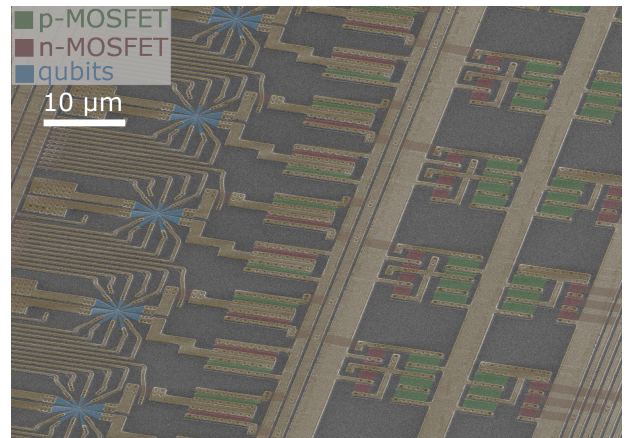


FIG. 1. False colored SEM micrograph of a planar cryogenic quantum IC (SemiQon Technologies) for interfacing of SiMOS qubit devices, containing digital CMOS logic blocks and quantum devices. MOSFET devices from the IC blocks, highlighted in green and red, are characterized in this work.

* nikolai.yurttagul@semiqaon.tech

† janne.lehtinen@semiqaon.tech

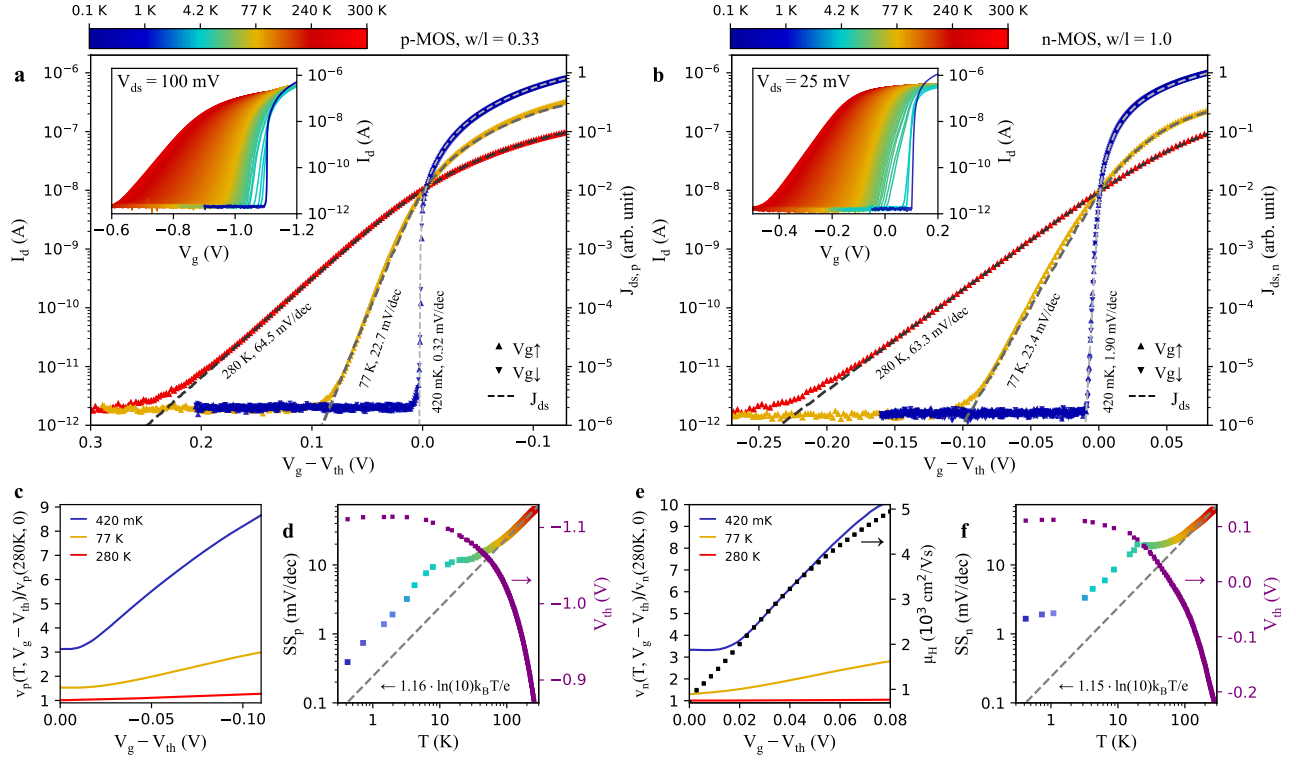


FIG. 2. FD-SOI MOSFET transport at variable temperature, $I_d(V_g)$ transfer characteristics for a p-MOSFET (a, $V_{ds} = 100$ mV), and an n-MOSFET (b, $V_{ds} = 25$ mV) between 280 K and 420 mK. The arrows in the legend indicate the sweep direction of V_g (see also Fig. 3 for details). Raw data is plotted in the inset panels and transfer characteristics at 420 mK, 77 K, and 280 K is highlighted in the main panel. The curves in the main panel are fitted to Eq. 3 ($J_{ds,i}$, arb. unit) to extract SS_i , and v_i . c,e: $v_i(V_g)$ above threshold, all values are normalized to the subthreshold value at 280 K. In e the measured mobility for a n-Hall-bar with the same C_{ox} is plotted for comparison. d,f: $SS(T)$ and $V_{th}(T)$ plotted against temperature. Adjusted thermionic limits $SS_i(T) = s_i \log(10) k_B T / e$ are plotted with dashed lines for comparison.

and SiMOS-qubits (Fig. 1). The gate stack fabrication is tailored to sub-1 K applications, such that a low impurity density facilitates low charge noise. For these gate-stacks a combination of very low $1/f$ noise with record low SS of 4 mV/dec at 5.6 K was already demonstrated earlier, consistent over a range of physical gate length from 50 nm to several μm [26]. In this work we evaluate the switching behaviour of our cryo-MOSFETs down to 420 mK and show by measuring gate transfer characteristics that ~ 1 mV/dec switching in Si MOSFETs is possible at millikelvin temperatures, enabling ultra-low power operation of millikelvin cryo-CMOS.

MOSFETs were manufactured by SemiQon Technologies on 150 mm SOI wafers. In these, charge carriers are extended from doped contact regions into a 20 nm thick intrinsic channel, which can be tuned by a front-gate and back-gate. Cryogenic characterization was performed with ^3He evaporation cooling in a cryogen free system (Bluefors LD250HE) with 420 mK base temperature. Source and gate potentials were controlled using isolated ultra-low noise high-stability voltage sources (Quantum Machines, QDAC-II). Source and drain current was measured with a low-noise high-stability tran-

simpedance amplifier (Basel instruments SP983c). The input JFET of the preamplifier has a leakage current of about 2 pA, which sets the current floor in all shown $I_d(V_g)$ -sets.

To quantify switching metrics of our MOSFETs we sweep V_g and measure I_d at temperature T and source-drain voltage V_{ds} . We extract SS by fitting the log-linear part of $I_d(V_g)$, and use a phenomenological approach to fit $I_d(V_g)$ over the full interval of V_g . For this we calculate the carrier density of carrier type $i = n, p$ with

$$n_i(\Psi_S) = \int_{-\infty}^{\infty} f(E) N_i^{2D}(E, \Psi_S) dE. \quad (1)$$

Ψ_S is the surface potential, $f(E) = (e^{(E-E_F)/k_B T} + 1)^{-1}$ is the Fermi-Dirac distribution, N_i^{2D} is the two-dimensional density of states which is constant above the band edge $E_i = E_i^0 \pm e\Psi_S$. V_g is the sum of the voltage drop over the gate oxide and the semiconductor as [12]

$$V_{g,i} = \Psi_S + n_i(\Psi_S) e / C_{ox}. \quad (2)$$

$C_{ox} = \epsilon/t$ is the geometric gate capacitance where ϵ is the static permittivity and t is the thickness of the gate

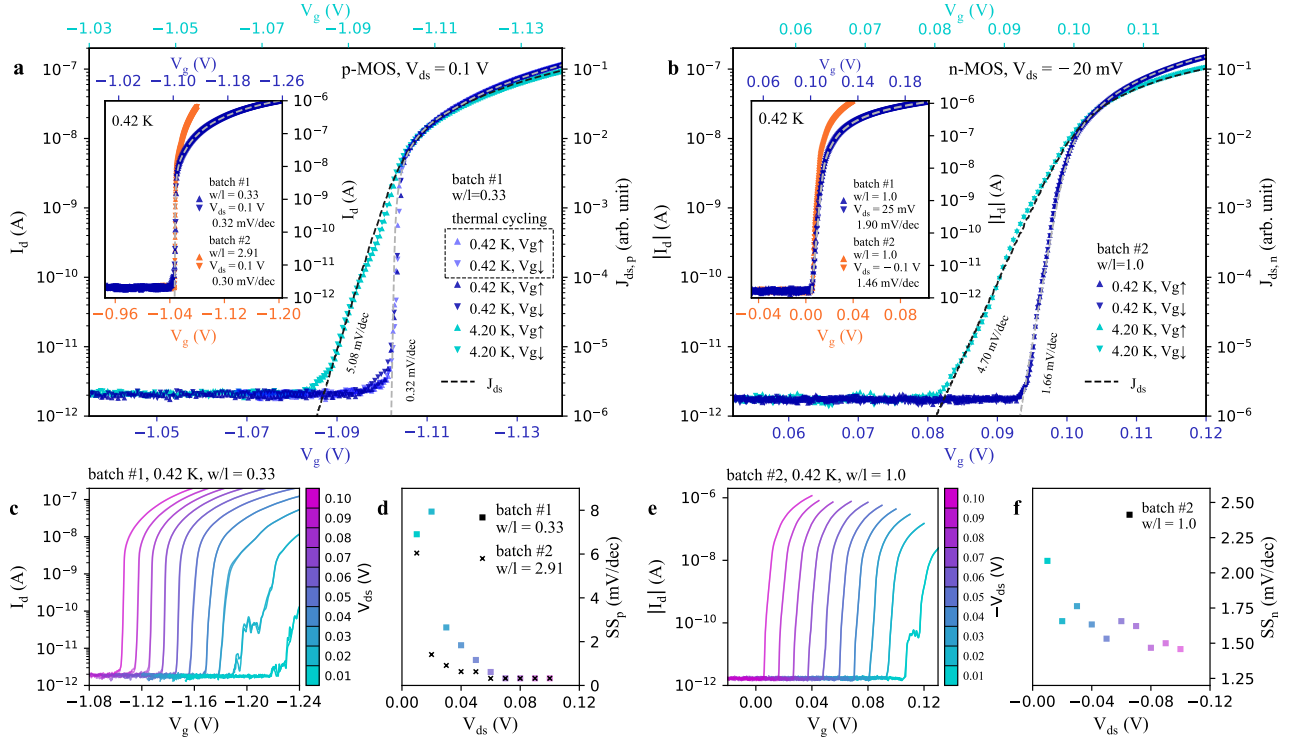


FIG. 3. Sub-Kelvin FD-SOI MOSFET transport, $I_d(V_g)$ transfer characteristics for a p-MOSFET (a, $V_{ds} = 100$ mV), and an n-MOSFET (b, $V_{ds} = -20$ mV) at 420 mK and 4.2 K. The arrows in the legend indicate the sweep direction of V_g . Inset of a: $I_d(V_g)$ of two p-MOSFETs are from different wafer batches with different channel width to gate length ratio w/l . Inset of b: $I_d(V_g)$ of two n-MOSFETs that are from different wafer batches with the same w/l but different V_{ds} magnitude and polarity. c,e $I_d(V_g)$ transfer characteristics are measured at 420 mK at variable V_{ds} . d,f $SS(V_{ds})$ at 420 mK extracted by fitting $I_d(V_g)$ in the subthreshold region.

dielectric. As in [14, 21] we account for subgap states by adding a broadened band edge $N_i(E) = N_i^{2D} e^{(E \pm E_i)/E_{w,i}}$ for $E < E_i$, with the decay energy $E_{w,i}$ [21]. We fit measured $I_d(V_g)$ transfer characteristics to a phenomenological source-drain current density

$$J_{ds,i} = v_i q_i \quad (3)$$

with $q_i = en_i(V_g)$. The transport parameter v_i is used to account for a relative change in carrier mobility with density and temperature.

We benchmark the switching performance of our MOSFETs in a range from 280 K to 420 mK. Results for a typical p-MOSFET and an n-MOSFET are depicted in Fig. 2. In Fig. 2, a and b we plot selected $I_d(V_g - V_{th})$ at 280 K, liquid N_2 temperature 77 K, and 420 mK to showcase the significant change in turn-on when cooling over this wide temperature range. V_{th} is the threshold voltage with $I_d(V_g \leq V_{th}) \leq 10^{-8}$ A. By fitting the log-linear subthreshold current we find the expected linear decrease in SS with decreasing temperature, $SS(T) = s_i \log(10) k_B T / e$, with $s_p = 1.16$ down to about 100 K, and $s_n = 1.15$ down to about 150 K (Fig. 2, d and f). At lower temperatures the measured SS does not follow a linear temperature dependence but plateaus between 10 K and 20 K. Notably, by cooling further we find SS

further decreasing linearly for both electrons and holes, reaching 0.32 mV/dec at 420 mK for the p-MOSFET, while forming a second plateau between 1-2 mV/dec for the n-MOSFET below 2 K. At 4.2 K we find 5.1 mV/dec for the p-MOSFET and 4.5 mV/dec for the n-MOSFET (Fig. 2, d and f), well reproducing previous results from different wafer batches, found to be consistent in gate length from 50 nm to >1 μm [26]. Regarding the form of $SS_p(T)$ at all T , and $SS_n(T)$ above 3 K, our results are in agreement with the findings in [21].

Besides the improvement in SS , the on-current for both MOSFETs increases by a decade when cooling from 280 K to 420 mK (Fig. 2, a and b). Fitting v_i (Fig. 2, c and e) above threshold accounts for this relative increase in J_{ds} which is not caused by a change in carrier density with increasing V_g alone. In Fig. 2, e we compare v_n at 420 mK to the measured electron mobility μ_H of an n-Hall-bar MOS-test structure with identical C_{ox} at 420 mK. We note that the increase in electron mobility above threshold qualitatively reproduces the increase in v_n over the measured interval of V_g .

At 420 mK we evaluate the switching behaviour of our MOSFETs with respect to hysteresis or transport features originating from single-electron tunneling [22] or delocalization of charge carriers [25]. For this we measure

$I_d(V_g, V_{ds})$ characteristics of our MOSFETs by sweeping V_g back and forth at variable V_{ds} (Fig. 3, c and e). As reference we characterize a device from another wafer batch, with the same w/l (n-MOS), and a 9 times larger w/l (p-MOS). For all devices we find no hysteresis, current jumps, or current oscillations down to $V_{ds} = 20$ mV, except only the p-MOSFET with $w/l = 0.33$ showing oscillatory current modulation at $V_{ds} = 20$ mV. We find very similar switching behaviour between the devices from different wafer batches, with 1.66 mV/dec at $V_{ds} = -20$ mV versus 1.90 mV/dec at $V_{ds} = 25$ mV for the n-MOSFETs (Fig. 2, b versus Fig. 3, b), and 0.32 mV/dec versus 0.30 mV/dec for the p-MOSFETs (Fig. 3, a, inset). In the latter, the expected increase in on-current due to the increased w/l can be seen as well. We further probe the sub-1 mV/dec hole turn-on by doing full thermal cycling which does not result in a change of subthreshold swing or threshold voltage (Fig. 3, a). We note that for both electrons and holes we achieve SS below the lowest reported value of 3.5 mV/dec at 420 mK [21].

The very sharp turn-on of our MOSFETs enables lowering the supply voltage V_{dd} in cryo-CMOS ICs well below that of state-of-the-art FD-SOI, which is currently above 0.4 V [27] and typically over 1 V. When switching from $I_{off} = V_{DS}(V_g = 0, V_{ds} = V_{dd})$ to $I_{on} = I_{ds}(V_g = V_{ds} = V_{dd})$ over several decades in current, our MOSFETs can be switched on with V_{dd} of the order of tens of millivolts leading to reduction of dynamic power-loss by more than a factor of hundred compared to the state-of-the-art.

In order to discuss the expected power loss of a CMOS IC operating with millikelvin MOSFETs we depict an inverter (Fig. 4) with load capacitance C_l , driven by a square wave at frequency f and amplitude V_{dd} . The dynamic power consumption per channel unit area is

$$P_d = C_{ox} V_{dd}^2 f. \quad (4)$$

In a real system we also have to take into account the frequency cutoff imposed by the finite charging and discharging delay of the output voltage response $V_{out} = V_{ds}(1 - e^{-t/R_i C_{tot}})$, where $R_i(V_{dd})$ is the n- or p-MOSFET resistance. This limits the maximum operation frequency to $f_{max} = 1/\tau_R + 1/\tau_F$, with the rise and fall time τ_R and τ_F . In Fig. 4 we plot the dynamic power loss and limit frequency for selected values of V_{dd} , assuming a turn-on characteristics as measured on our MOSFETs (Fig. 2, Fig. 3). For the calculation we have assumed an output load of three transistor gates as $C_{tot} = C_g + C_l = 4C_g$, which corresponds to a typical fan-out for a realistic CMOS IC. We have neglected inductive loads and assumed that the circuit operates between 10 % (off) and 90 % (on) V_{dd} . Notably, even for 40 mV supply voltage, the realistic operation frequency is still about 1 GHz for our devices. A qubit controller, consisting of MOSFETs with $w/l = 100$ nm/30 nm, driven with 500 MHz, would only dissipate 2 pW per MOSFET. This can be compared to the cooling

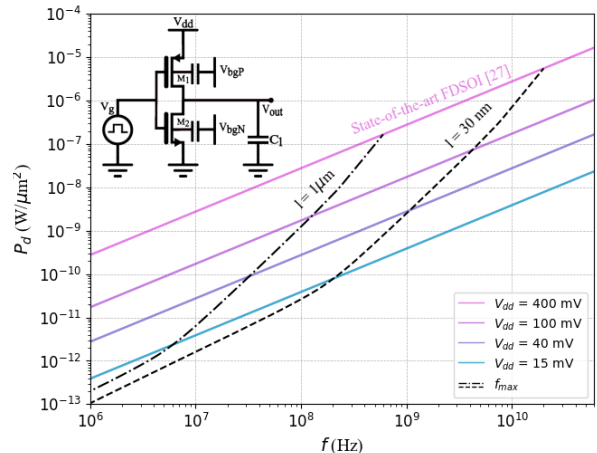


FIG. 4. Dynamic power consumption per unit channel area versus frequency at selected V_{dd} . The dash-dotted ($l = 1$ μm) and the dashed ($l = 30$ nm) lines indicate the maximum circuit operation frequency for an inverter (circuit left top corner) with load capacitance $C_l = 3C_g$. V_{bgN} and V_{bgP} are back-gates for aligning the threshold voltages of M2 and M1.

power of a conventional dilution refrigerator at 50 mK, which is as high as 100 μW , while ^3He evaporation or dilution refrigeration at 500 mK can provide a cooling power of several tens of mW. This showcases that integrated circuits, containing of up to $10^7 - 10^{10}$ of these MOSFETs are possible at millikelvin temperatures.

In summary, we have characterized cryogenic FD-SOI MOSFETs produced on a CMOS pilot-line and shown that the improvement in switching metrics, due to reduced thermal excitations of charge carriers, can be harnessed down to the millikelvin temperature regime. This advancement can solve the power dissipation bottleneck, limiting very large-scale integration of CMOS circuits at ultra-low temperatures, and enable all-cryogenic control of quantum circuits, which is a prerequisite for fault-tolerant quantum computation.

Acknowledgements: This research was funded by the European Union's Horizon EIC programme under grant agreement No. 101136793 (SCALLOP) and Chips Joint Undertaking programme under grant agreement No. 101139908 (ARCTIC) and Business Finland project 10200/31/2022 (ToScaleQC).

-
- [1] R. Saligram, A. Raychowdhury, and S. Datta, The future is frozen: cryogenic cmos for high-performance computing, *Chip* **3**, 100082 (2024).
 - [2] R. Saligram, D. Prasad, D. Pietromonaco, A. Raychowdhury, and B. Cline, A 64-bit arm cpu at cryogenic temperatures: Design technology co-optimization for power

- and performance, in *2021 IEEE Custom Integrated Circuits Conference (CICC)* (2021) pp. 1–2.
- [3] H. L. Chiang, T. C. Chen, J. F. Wang, S. Mukhopadhyay, W. K. Lee, C. L. Chen, W. S. Khwa, B. Pulicherla, P. J. Liao, K. W. Su, K. F. Yu, T. Wang, H. S. P. Wong, C. H. Diaz, and J. Cai, Cold cmos as a power-performance-reliability booster for advanced finfets, in *2020 IEEE Symposium on VLSI Technology* (2020) pp. 1–2.
 - [4] S. J. Pauka, K. Das, R. Kalra, A. Moini, Y. Yang, M. Trainer, A. Bousquet, C. Cantaloube, N. Dick, G. C. Gardner, M. J. Manfra, and D. J. Reilly, A cryogenic cmos chip for generating control signals for multiple qubits, *Nature Electronics* **4**, 64 (2021).
 - [5] H. Oka, Cryo-cmos device technology for quantum computers, *JSAP Review* **2022**, 220305 (2022).
 - [6] D. Underwood, J. A. Glick, K. Inoue, D. J. Frank, J. Timmerwilke, E. Pritchett, S. Chakraborty, K. Tien, M. Yeck, J. F. Bulzacchelli, C. Baks, R. Robertazzi, M. Beck, R. V. Joshi, D. Wisnieff, S. Lekuch, B. P. Gaucher, D. J. Friedman, P. Rosno, D. Ramirez, and J. Ruedinger, Using cryogenic cmos control electronics to enable a two-qubit cross-resonance gate, *PRX Quantum* **5**, 010326 (2024).
 - [7] O. Saint-Pe, M. Tulet, R. Davancens, F. Larnaudie, P. Magnan, P. Martin-Gonthier, F. Corbiere, and M. Estriebeau, Space optical instruments design optimisation thanks to CMOS image sensor technology, in *Sensors, Systems, and Next-Generation Satellites IX*, Vol. 5978, edited by R. Meynart, S. P. Neeck, and H. Shimoda, International Society for Optics and Photonics (SPIE, 2005) p. 597811.
 - [8] X. Xue, B. Patra, J. P. G. van Dijk, N. Samkharadze, S. Subramanian, A. Corna, B. Paquelet Wuetz, C. Jeon, F. Sheikh, E. Juarez-Hernandez, B. P. Esparza, H. Ramapurawala, B. Carlton, S. Ravikumar, C. Nieva, S. Kim, H.-J. Lee, A. Sammak, G. Scappucci, M. Veldhorst, F. Sebastiano, M. Babaie, S. Pellerano, E. Charbon, and L. M. K. Vandersypen, Cmos-based cryogenic control of silicon quantum circuits, *Nature* **593**, 205 (2021).
 - [9] H.-C. Han, F. Jazaeri, A. D'Amico, A. Baschiroto, E. Charbon, and C. Enz, Cryogenic characterization of 16 nm finfet technology for quantum computing, in *ESSCIRC 2021 - IEEE 47th European Solid State Circuits Conference (ESSCIRC)* (2021) pp. 71–74.
 - [10] M. D. Michielis, E. Ferraro, E. Prati, L. Hutin, B. Bertrand, E. Charbon, D. J. Ibberson, and M. F. Gonzalez-Zalba, Silicon spin qubits from laboratory to industry, *Journal of Physics D: Applied Physics* **56**, 363001 (2023).
 - [11] F. Pobell, *Matter and Methods at Low Temperatures* (World Scientific, 2007).
 - [12] M. Lundstrom, *Fundamentals of Nanotransistors* (World Scientific, 2007).
 - [13] A. Beckers, F. Jazaeri, and C. Enz, Theoretical limit of low temperature subthreshold swing in field-effect transistors, *IEEE Electron Device Letters* **41**, 276 (2020).
 - [14] H. Bohuslavskyi, A. G. M. Jansen, S. Barraud, V. Barral, M. Cassé, L. Le Guevel, X. Jehl, L. Hutin, B. Bertrand, G. Billiot, G. Pillonnet, F. Arnaud, P. Galy, S. De Franceschi, M. Vinet, and M. Sanquer, Cryogenic subthreshold swing saturation in fd-soi mosfets described with band broadening, *IEEE Electron Device Letters* **40**, 784 (2019).
 - [15] A. Beckers, F. Jazaeri, and C. Enz, Characterization and modeling of 28-nm bulk cmos technology down to 4.2 k, *IEEE Journal of the Electron Devices Society* **6**, 1007 (2018).
 - [16] R. M. Incandela, L. Song, H. Homulle, E. Charbon, A. Vladimirescu, and F. Sebastiano, Characterization and compact modeling of nanometer cmos transistors at deep-cryogenic temperatures, *IEEE Journal of the Electron Devices Society* **6**, 996 (2018).
 - [17] R. M. Incandela, L. Song, H. Homulle, F. Sebastiano, E. Charbon, and A. Vladimirescu, Nanometer cmos characterization and compact modeling at deep-cryogenic temperatures, in *2017 47th European Solid-State Device Research Conference (ESSDERC)* (2017) pp. 58–61.
 - [18] F. Balestra and G. Ghibaudo, Physics and performance of nanoscale semiconductor devices at cryogenic temperatures, *Semiconductor Science and Technology* **32**, 023002 (2017).
 - [19] B. C. Paz, L. Le Guevel, M. Cassé, G. Billiot, G. Pillonnet, A. G. M. Jansen, R. Maurand, S. Haendler, A. Juge, E. Vincent, P. Galy, G. Ghibaudo, M. Vinet, S. de Franceschi, T. Meunier, and F. Gaillard, Variability evaluation of 28nm fd-soi technology at cryogenic temperatures down to 100mk for quantum computing, in *2020 IEEE Symposium on VLSI Technology* (2020) pp. 1–2.
 - [20] A. Chabane, M. Prathapan, P. Mueller, E. Cha, P. A. Francese, M. Kossel, T. Morf, and C. Zota, Cryogenic characterization and modeling of 14 nm bulk finfet technology, in *ESSCIRC 2021 - IEEE 47th European Solid State Circuits Conference (ESSCIRC)* (2021) pp. 67–70.
 - [21] H. Oka, H. Asai, T. Inaba, S. Shitakata, H. Yui, H. Fuketa, S. Iizuka, K. Kato, T. Nakayama, and T. Mori, Milli-kelvin analysis revealing the role of band-edge states in cryogenic mosfets, in *2023 International Electron Devices Meeting (IEDM)* (2023) pp. 1–4.
 - [22] S. Pati Tripathi, S. Bonen, A. Bharadwaj, T. Jager, C. Nastase, S. Iordănescu, G. Boldeiu, M. Pășteanu, A. Nicoloiu, I. Zdru, A. Müller, and S. P. Voinigescu, Characterization and modeling of quantum dot behavior in fdsoi devices, *IEEE Journal of the Electron Devices Society* **10**, 600 (2022).
 - [23] T.-Y. Yang, A. Ruffino, J. Michniewicz, Y. Peng, E. Charbon, and M. F. Gonzalez-Zalba, Quantum transport in 40-nm mosfets at deep-cryogenic temperatures, *IEEE Electron Device Letters* **41**, 981 (2020).
 - [24] S. Bonen, M. Sadegh Dadash, A. Zandieh, U. Alakuşu, M. Jia Gong, J. Rafique, L. Wu, E. Checca, H. Yun Hsu, S. Pati Tripathi, G. Cooke, and S. P. Voinigescu, Harnessing the unique features of fdsoi cmos technology in fibre-optic, millimetre-wave, and quantum computing circuits from 2 k to 400 k, *Solid-State Electronics* **194**, 108343 (2022).
 - [25] A. A. Shashkin and S. V. Kravchenko, Recent developments in the field of the metal-insulator transition in two dimensions, *Applied Sciences* **9**, 10.3390/app9061169 (2019).
 - [26] H. Bohuslavskyi, A. Ronzani, J. Härtinen, A. Rantala, A. Shchepetov, P. Koppinen, J. S. Lehtinen, and M. Prunnila, Scalable on-chip multiplexing of silicon single and double quantum dots (2024), arXiv:2208.12131 [cond-mat.mes-hall].
 - [27] GlobalFoundries, <https://gf.com/technology-platforms/fdx-fd-soi/> (2024).